Proceedings of the 10th Workshop on Quantum Chaos and Localisation Phenomena (CHAOS 21)

Some Applications of Generalized Euler Characteristic of Quantum Graphs and Microwave Networks

S. Bauch[a,*], M. Ławniczak[a], J. Wrochna[a], P. Kurasov[b] and L. Sirko[a]

[a] *Institute of Physics, Polish Academy of Sciences, Aleja Lotników 32/46, 02-668 Warszawa, Poland*
[b] *Department of Mathematics, Stockholm University, S-106 91 Stockholm, Sweden*

Doi: 10.12693/APhysPolA.140.525 *e-mail: bauch@ifpan.edu.pl

In this article we continue to explore the possibilities offered by our discovery that one of the main graph and network characteristic, the generalized Euler characteristic χ_G, can be determined from a graph/network spectrum. We show that using the generalized Euler characteristic χ_G the number of vertices with Dirichlet $|V_D|$ boundary conditions of a family of graphs/networks created on the basis of the standard quantum graphs or microwave networks can be easily identified. We also present a new application of the generalized Euler characteristic for checking the completeness of graphs/networks spectra in the low energy range.

topics: quantum graphs, Euler characteristic, boundary conditions, microwave networks

1. Introduction

The concept of a graph was introduced by Leonhard Euler in XVIII century [1]. Exactly two hundred years later, Linus Pauling published an article [2] in which he used graphs to describe the motion of quantum particles in a physical network. This approach is called quantum graph model and is widely used to investigate many physical systems, e.g. mesoscopic quantum system [3, 4], quantum wires [5] and optical wave guides [6]. Richard P. Feynman [7] applied diagrams (graphs) as pictorial representation of the mathematical expressions describing the behavior and interaction of subatomic particles. Due to the extremely wide range of applications the theory of quantum graphs has been the subject of extensive research so far [8–14]. In particular, Kottos and Smilansky [9] showed that quantum graphs can be used to study quantum chaos, i.e., the phenomena found in quantum systems that are chaotic at the classical limit.

The metric graph $\Gamma = (V, E)$ consists of vertices $v \in V$ connected by edges $e \in E$ being intervals of the length l_e on the real line $\mathbb{R}$. The Laplace operator $L(\Gamma) = -\frac{\mathrm{d}^2}{\mathrm{d}x^2}$ acting in the Hilbert space of square integrable functions is unambiguously determined by the graph. The Laplace operator $L(\Gamma)$ is self-adjoint and has a discrete and non-negative spectrum [12]. If all graph vertices V have standard (called also natural, Kirchhoff, Neumann) boundary conditions, i.e. functions are continuous at vertices and the sums of their oriented derivatives at vertices are zero, then the Laplacian has a simple zero eigenvalue with the eigenfunction being a constant. When even one vertex V_D of the graph has the Dirichlet boundary condition (functions is zero at the vertex) then spectral multiplicity of the eigenvalue of 0 becomes zero instead of one, provided the graph is connected.

The most important characteristic of metric graphs $\Gamma = (V, E)$ are the total length $\mathcal{L} = \sum_{e \in E} l_e$ and the Euler characteristic $\chi = |V| - |E|$, where $|V|$ and $|E|$ denote the number of vertices and edges. The later one is a purely topological quantity, but as we have shown in [15–17] and [18], it can be also obtained from the graph spectrum.

The microwave networks simulating quantum graphs [19–25], which is possible thanks to the formal analogy of the one-dimensional Schrödinger equation describing quantum graphs and the telegrapher's equation for microwave networks [19, 22], were used in experiments to obtain graph spectra, while the pseudo orbits method developed in [26] was applied in numerical calculation of them. It should be emphasized that microwave networks are the only ones that allow experimental simulations of quantum systems with all three types of symmetry within the framework of the random matrix theory (RMT). These symmetries are: Gaussian orthogonal ensemble (GOE) — systems with preserved time reversal symmetry (TRS) [17, 19–21, 23, 27, 28], Gaussian symplectic

ensemble (GSE) — systems with TRS and half-spin [29], and Gaussian unitary ensemble (GUE) — systems with broken TRS [19, 24, 30–33]. The examples of the other model systems often used in simulations of complex quantum systems with TRS are flat microwave billiards [34–50] and atoms in strong microwave fields [51–63].

2. Theoretical outline

As mentioned in Sect. 1, the most important characteristics of a metric graph are the total length

$$\mathcal{L} = \sum_{e \in E} l_e \tag{1}$$

and the Euler characteristic

$$\chi = |V| - |E|. \tag{2}$$

The total length $\mathcal{L}$ gives the eigenvalues of a graph λ_n via Weyl's formula

$$\lambda_n = \left(\frac{\pi}{\mathcal{L}}\right)^2 n^2 + \mathcal{O}(n), \tag{3}$$

where $\mathcal{O}(n)$ is a function which in the limit $n \to +\infty$ is bounded by a constant.

The Euler characteristic χ is related to the first Betti number β describing the number of independent cycles in the graph:

$$\beta = |E| - |V| + 1 \equiv 1 - \chi. \tag{4}$$

This number is equal to the number of edges that must be removed from the connected graph in order to turn it into a tree graph.

In our previous articles [17, 18], we derived formulas for the Euler characteristic for graphs with only standard boundary conditions (SBC) at the vertices and with mixed, standard and Dirichlet boundary conditions (DBC) at vertices. In the case of standard boundary conditions

$$\chi = 2 + 8\pi^2 \sum_{\substack{k_n \in \Sigma(L^{\mathrm{st}}(\Gamma)) \\ k_n \neq 0}} \left. \frac{\sin(\frac{k_n}{t})}{\left(\frac{k_n}{t}\right)\left[(2\pi)^2 - \left(\frac{k_n}{t}\right)^2\right]} \right|_{t \geq t_0}, \tag{5}$$

where $\Sigma(L^{\mathrm{st}}(\Gamma))$ denotes the spectrum of the Laplacian $L^{\mathrm{st}}(\Gamma)$ with standard vertex conditions taken in the square root scale, i.e., the numbers k_n are the square roots of the eigenenergies λ_n, and t is a scaling parameter [15–17] with $t_0 = 1/(2l_{\min})$, where $l_{\min}$ is the length of the shortest edge of the graph.

For graphs and networks with Dirichlet boundary conditions

$$\chi_G := \chi - |V_D| = 8\pi^2 \sum_{k_n \in \Sigma(L^{\mathrm{st,D}}(\Gamma))} \left. \frac{\sin(\frac{k_n}{t})}{\left(\frac{k_n}{t}\right)\left[(2\pi)^2 - \left(\frac{k_n}{t}\right)^2\right]} \right|_{t \geq t_0}. \tag{6}$$

Here, $\Sigma(L^{\mathrm{st,D}}(\Gamma))$ denotes the spectrum of the Laplacian $L^{\mathrm{st,D}}(\Gamma)$ with standard and the Dirichlet vertex conditions. In (6), we assume that $|V_D| \neq 0$.

These two formulas can be written in a single elegant form

$$\mathcal{E}(|V_D|) = 2\delta_{(0,|V_D|)} + 8\pi^2 \sum_{\substack{k_n \in \Sigma(L(\Gamma)) \\ k_n \neq 0}} \left. \frac{\sin(\frac{k_n}{t})}{\left(\frac{k_n}{t}\right)\left[(2\pi)^2 - \left(\frac{k_n}{t}\right)^2\right]} \right|_{t \geq t_0}, \tag{7}$$

where $\delta_{(i,j)}$ is the Kronecker delta. Depending on the boundary conditions, $\Sigma(L(\Gamma))$ denotes either the spectrum of the Laplacian $L^{\mathrm{st}}(\Gamma)$ or $L^{\mathrm{st,D}}(\Gamma)$.

The new formula for the generalized Euler characteristic $\mathcal{E}(|V_D|)$ includes also the case $|V_D| = 0$ and for the limited cases $|V_D| = 0$ and $|V_D| \neq 0$, $\mathcal{E}(|V_D| = 0) = \chi$ and $\mathcal{E}(|V_D| \neq 0) = \chi_G$, respectively.

Formally, obtaining the quantities $\mathcal{L}$ from Weyl's formula and $\mathcal{E}(|V_D|)$ from (7), requires the knowledge of the whole sequence of eigenvalues [15, 16]. We proved in [17, 18] and confirmed in [64, 65] that the Euler characteristic can be evaluated using only limited number $K = K_{\min}$ of the lowest eigenvalues (resonances)

$$K \geq |V| + 2\mathcal{L}t \left(1 - \exp\left(-\frac{\epsilon\pi}{\mathcal{L}t}\right)\right)^{-\frac{1}{2}}, \tag{8}$$

where $|V|$ is the total number of graph vertices, ϵ is the accuracy of determining the Euler characteristic from (7). To obtain the smallest possible number of resonances $K_{\min}$, for a given accuracy ϵ, we assign to t its smallest allowed value $t = t_0$. Since the Euler characteristic is an integer, the accuracy of its determination should be taken $\epsilon < 1/2$. In our calculations of $K_{\min}$ we will assume $\epsilon = 1/4$. Then, the approximated formula for $\mathcal{E}(|V_D|)$ becomes

$$\mathcal{E}(|V_D|, t) = 2\delta_{(0,|V_D|)} + 8\pi^2 \sum_{n=1}^{K_{\min}} \frac{\sin(\frac{k_n}{t})}{\left(\frac{k_n}{t}\right)\left[(2\pi)^2 - \left(\frac{k_n}{t}\right)^2\right]}, \tag{9}$$

and should reach a plateau within the limits $\pm\frac{1}{4}$ of the value of Euler characteristic $\mathcal{E}(|V_D|)$ for $t_0 \leq t \leq t_{\max}$ (see Figs. 1 and 2), where $t_{\max} \simeq \sqrt[3]{4} t_0$ [18].

3. Experimental setup and methodology of measurements

To measure spectra of microwave networks necessary to calculate their Euler characteristic, we used the set-up that is standard for such experiments (see, e.g. [66]). It consists of the Agilent E8364B vector network analyzer (VNA) and the HP 85133-616 high class flexible microwave cable that connects the VNA with the measured network and is equivalent to attaching an infinite lead to the quantum graph [27]. The schemes of the considered graph and the microwave network are shown in insets in Figs. 1 and 2. The VNA was calibrated using the Agilent 4691-60004 electronic calibration module to eliminate impact of network external elements on the measurement results.

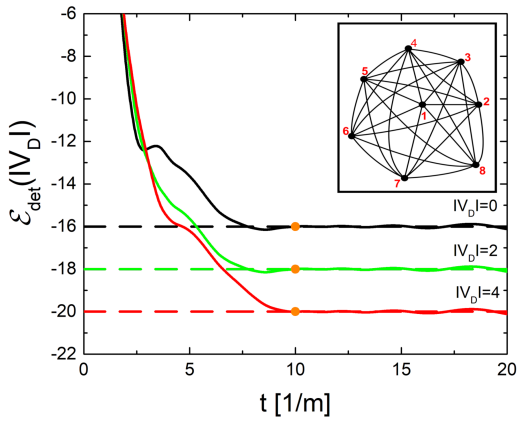

Fig. 1. The generalized Euler characteristic $\mathcal{E}_{\rm det}(|V_D|)$ calculated for the graphs $\Gamma = (12, 28, 4)$, $\Gamma = (12, 28, 2)$, and $\Gamma = (12, 28, 0)$, are denoted by red, green, and black solid lines, respectively. The numerical calculations are compared to the theoretical predictions marked by dashed lines. The parameter $t_0 = 10$ m^{-1}, used in (8) is marked by orange full circles. The scheme of the graph is shown in the inset.

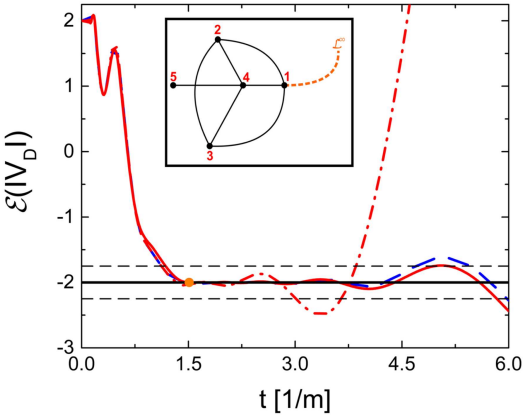

Fig. 2. The generalized Euler characteristic $\mathcal{E}(|V_D|)$ as a function of the parameter t for microwave networks $\Gamma(5, 7, |V_D| = 0)$. The red dash-dot and solid line denote experimental results for $K_{\rm min} = 32$ and $K = 66$ resonances. The blue solid line represents numerical calculations for $K = 66$ resonances. The orange full circle marks $t_0 = 1.51$ m^{-1}, used in (8). The horizontal solid line represents the theoretical value of the Euler characteristic and the dashed lines show $\epsilon = \pm 1/4$ error limits. The scheme of the network with a lead connecting it to VNA is shown in the inset.

Microwave networks simulating quantum graphs are constructed with microwave coaxial cables and junctions that correspond to the edges and vertices of the graphs. The microwave cables consist of an outer conductor with an inner radius $r_2 = 0.15$ cm and an inner conductor of a radius $r_1 = 0.05$ cm surrounded by the dielectric material (teflon). The cut-off frequency of the TE$_{11}$ mode below which only the fundamental TEM can propagate in the cable [67, 68] is $\upsilon_{\rm cut} = \frac{c}{\pi(r_1+r_2)\sqrt{\varepsilon}} = 33$ GHz, where the dielectric constant of teflon $\varepsilon = 2.06$ was measured in our lab. The physical dimension of microwave networks is related to their optical length, i.e., is the dimension of the simulated quantum graphs by the relationship $l_{\rm opt} = \sqrt{\varepsilon} l_{ph}$.

The Agilent E8364B vector network analyzer provides the ability to perform one-port and two-port measurements of the scattering matrix $S(\nu)$. However, one-port measurements are preferable, if possible, because it means a smaller opening of the tested system to the environment, and thus a smaller width of the observed resonances. This, by reducing the overlap of resonances, facilitates the identification of the complete set of the eigenvalues, which is crucial in all experiments on the energy level correlations. The scattering matrix in the case of one-port measurements is defined as $S_{11}(\nu) = \sqrt{R(\nu)}\,{\rm e}^{{\rm i}\theta(\nu)}$, where $R(\nu)$ is the reflection coefficient and $\theta(\nu)$ is the phase of a signal.

4. Results

First, we present the results that are a continuation of the findings presented in [17, 18] on "hearing" the network/graph boundary conditions solely on the basis of its spectrum. Next, we show a new application of the generalized Euler characteristic to check the completeness of networks/graphs spectra in the range of low energies.

4.1. Hearing the boundary conditions of graphs emerging from standard quantum graphs

The fully connected (complete) quantum graphs are characterized by the strict relation between the number of their edges $|E|$ and vertices $|V|$, i.e.,

$$|E| = \frac{1}{2}|V|\big(|V| - 1\big). \tag{10}$$

Moreover, by definition, the Dirichlet boundary conditions are excluded in these graphs. In [17], we showed that for such graphs it is enough to evaluate the Euler characteristic from a graph spectrum to learn whether it is a complete graph and how many vertices/edges it has. This is possible because

$$|V| = \frac{3 + \sqrt{9 - 8\chi}}{2} \tag{11}$$

gives an integer for the complete graphs.

Here, we will analyze a detaching transformation which leads from a standard original graph to the one which may posses, in general, the Neumann [18] and Dirichlet boundary conditions. A standard quantum graph possesses only vertices with the standard boundary conditions. The following notation will be used for a short description of graphs: $\Gamma(|V|, |E|, |V_D|)$, where $|V_D|$ is the number of vertices with the Dirichlet boundary condition, and $|V|$ and $|E|$ denote the total number of vertices and edges, respectively.

First, let us consider a transformation in which at least one edge $N_{\rm det}$ of the graph is detached from one of its vertices. We assume that the new graph remains connected. Then, the number of graph edges is preserved and $N_{\rm det} \geq 1$, new one-degree vertices appear in the graph. The number of new vertices, including the Neumann $|V_N|$ and the Dirichlet ones $|V_D|$, reads

$$|V_N| + |V_D| = N_{\rm det}. \tag{12}$$

The generalized Euler characteristic $\mathcal{E}_{\rm det}(|V_D|)$ of the new graph is given by

$$\mathcal{E}_{\rm det}(|V_D|) = \mathcal{E}_o(0) + N_{\rm det} - |V_D|, \tag{13}$$

where $\mathcal{E}_o(0)$ is the Euler characteristic of the original graph and $N_{det} - |V_D| = |V_N|$. Note that in this case the number of vertices of the new graph is increased by $N_{\rm det}$ but the number of its edges is preserved. Therefore, the number of the Dirichlet vertices $|V_D|$ can be found from

$$|V_D| = \mathcal{E}_o(0) - \mathcal{E}_{\rm det}(|V_D|) + N_{\rm det} \tag{14}$$

or equivalently

$$|V_N| = \mathcal{E}_{\rm det}(|V_D|) - \mathcal{E}_o(0). \tag{15}$$

Both (14) and (15) show that knowing the generalized Euler characteristic $\mathcal{E}_{\rm det}(|V_D|)$ and $\mathcal{E}_o(0)$ of the original graph, one can determine the number of graph vertices with the Dirichlet boundary conditions as well as with the Neumann boundary conditions (NBC).

The numerical calculation were performed for the complete graph $\Gamma(8, 28, 0)$ with $\mathcal{E}_o(0) = \chi = -20$. The results are presented in Fig. 1. The total optical length of the graph is $\mathcal{L} = 3.916$ m and the length of its shortest edge is $l_{\rm min} = 0.05$ m, giving $K_{\rm min} = 563$, which was estimated using (8). The generalized Euler characteristic $\mathcal{E}_{\rm det}(|V_D|)$ was calculated using (9). The graph $\Gamma(8, 28, 0)$ was the original for the following new graphs realizations, in which four, one plus three edges have been detached from two vertices:

(i) $N_{\rm det} = 4$ and all new four vertices have DBC,

(ii) $N_{\rm det} = 4$ and only 2 new vertices have DBC,

(ii) $N_{\rm det} = 4$ and all new vertices have NBC.

Then, according to (13), we have

$$\mathcal{E}_{\rm det}(|V_D|) = \begin{cases} -20 + (4-4) = \\ \quad -20 + 0 = -20, \ \text{for (i)}, \\ -20 + (4-2) = \\ \quad -20 + 2 = -18, \ \text{for (ii)}, \\ -20 + (4-0) = \\ \quad -20 + 4 = -16, \ \text{for (iii)} \end{cases} \tag{16}$$

graph realization.

In Fig. 1, red, green and black solid lines denote $\mathcal{E}_{\rm det}(|V_D|)$ for the graphs $\Gamma = (12, 28, 4)$, $\Gamma = (12, 28, 2)$, and $\Gamma = (12, 28, 0)$, respectively. The plateaux start at $t \simeq 10$ m^{-1}, which is very close to $t_0 = 10$ m^{-1}, marked in Fig. 1 by orange full circles, and are visible up to at least $t = 20$ m^{-1}. The numerical calculations are compared to the theoretical predictions marked in Fig. 1 by dashed lines. The agreement between them for $10 \leq t \leq 20$ m^{-1} is very good, however small deviations from them can be observed above $t_{\rm max} \simeq 1.6 t_0$. In the inset a scheme of the original graph is shown.

4.2. Missing levels and Euler characteristic

Microwave experiments on quantum chaos in which microwave objects, networks and cavities, simulate quantum graphs and billiards, yield the spectra of the studied systems. Quantum chaos manifests itself in statistical properties of the spectra. The completeness of the spectra is crucial for obtaining reliable results. Unfortunately, experimentally this happens rather seldom. Any method leading to the detection of the missing eigenvalues is highly desirable. There are several such methods, e.g. using Weyl's formula [69] and the power spectrum [32, 70, 71]. The Euler characteristic determined from the spectra, (5)–(7), and (9), turned out to be extremely sensitive to the loss of the lowest energy levels (resonances) in these spectra. By low energy levels we mean the levels with the numbers much smaller than $K_{\rm min}$. Especially, for small values of $K_{\rm min}$ this method, in contrast to the other ones, allows for quick determination of the frequency range in which a resonance is lost.

In order to present the dependence of the Euler characteristic on the position of the lost resonances we examined experimentally and numerically a microwave network simulating a quantum graph $\Gamma(5, 7, |V_D| = 0)$. The network of the total optical length $\mathcal{L} = 3.382$ m consists of five vertices and seven edges of lengths $l_{1,2} = 0.355$ m, $l_{1,3} = 0.436$ m, $l_{1,4} = 0.573$ m, $l_{2,3} = 0.391$ m, $l_{2,4}^{\rm min} = 0.331$ m ($t_0 = 1.51$ m^{-1}), $l_{3,4} = 0.341$ m, $l_{4,5} = 0.955$ m. The lower indexes are the numbers of vertices connected by the edge. The edge $l_{4,5}$ is the so called "tail" edge which can possess a single Neumann or Dirichlet vertex. In the latter case $|V_D| = 1$. The average number of resonances ΔN in the frequency range $\Delta\nu = 1$ GHz is $\Delta N = 2\Delta\nu\mathcal{L}/c \simeq 23$. The minimal number of resonances necessary to get the Euler characteristic with accuracy $\epsilon = \pm 1/4$ is $K_{\rm min} \simeq 32$, which corresponds to the frequency $\nu \simeq 1.418$ GHz.

We will consider only the network $\Gamma(5, 7, 0)$ with the "tail" edge having the vertex with NBC because the missing levels effect does not depend on the graph boundary conditions. The generalized Euler characteristic $\mathcal{E}(|V_D|)$ for this graph, $|V_D| = 0$, is $\mathcal{E}(0) = -2$. Its experimental spectrum in the frequency range 0–1 GHz is shown in Fig. 3.

The dependence of the generalized Euler characteristic $\mathcal{E}(|V_D|)$ on the parameter t together with the scheme of the network simulating the quantum

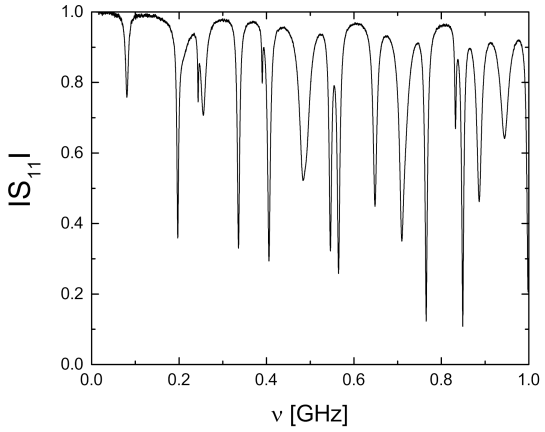

Fig. 3. The experimental spectrum obtained in a one-port measurement of the microwave network simulating quantum graph $\Gamma(5, 7, |V_D| = 0)$ in the frequency window 0–1 GHz.

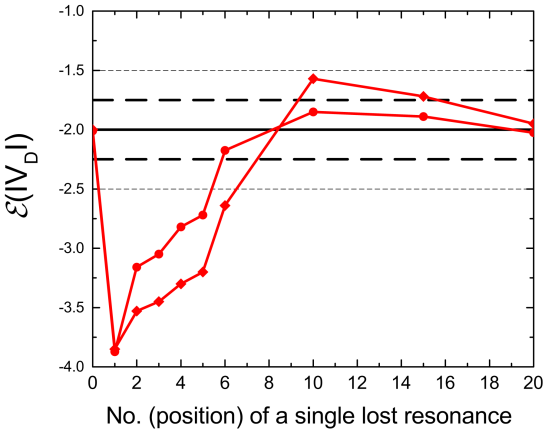

Fig. 4. The generalized Euler characteristic $\mathcal{E}(|V_D|)$ obtained from the experimental spectra of the $\Gamma(5, 7, 0)$ network as a function of the position (number) of the lost resonance. Solid red lines with full circles and with diamonds represent $\mathcal{E}(|V_D|)$ obtained using in (9) $K_{\min} = 32$ and $K = 66$ resonances, respectively. The horizontal solid line denotes $\chi = |V| - |E| = -2$, the horizontal thick dashed lines specify χ values within the accuracy limit $\epsilon = \pm 1/4$, while the thin dashed lines specify the maximum errors $\epsilon = \pm 1/2$ that allow for the correct determination of $\mathcal{E}(|V_D|)$.

graph $\Gamma(5, 7, |V_D| = 0)$ is shown in Fig. 2. The experimental results for $K_{\min} = 32$ resonances is shown by the red dash-dot line, whereas the experimental and numerical results for 66 resonances are shown as solid red line and blue dash line, respectively. The horizontal solid line represents the theoretical value of the Euler characteristic $\chi = |V| - |E|$ and the dashed lines show the $\epsilon = \pm 1/4$ error limits. The orange full circle marks $t_0 = 1.51$ m^{-1}, used in (8), where the beginning of the plateau is expected. The agreement with the theory and between the experimental and numerical results is excellent.

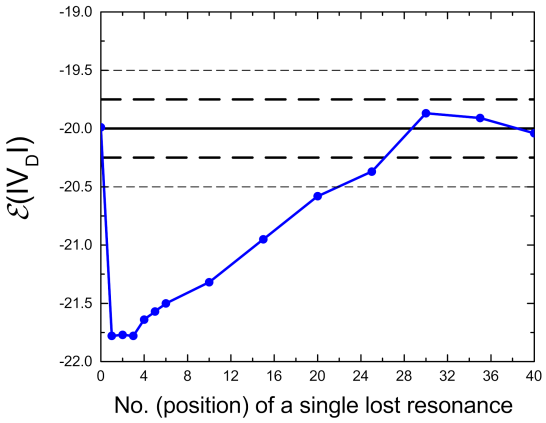

Fig. 5. The generalized Euler characteristic $\mathcal{E}(|V_D|)$ obtained numerically for the graph $\Gamma(8, 28, 0)$ as a function of the position (number) of the lost resonance. Solid blue lines with full circles represent $\mathcal{E}(|V_D|)$ obtained using in (9) $K_{\min} = 563$ resonances. The horizontal solid line denotes $\chi = |V| - |E| = -20$, the horizontal thick dashed lines specify the $\mathcal{E}(|V_D|)$ value within the accuracy limit $\epsilon = \pm 1/4$, while the thin dashed lines specify the maximum error $\epsilon = \pm 1/2$ that allows for the correct determination of $\mathcal{E}(|V_D|)$.

Figures 4 and 5 show changes of the generalized Euler characteristic $\mathcal{E}(|V_D|)$ as a function of the position (number) of the lost resonance. In Fig. 4, we present the experimental results for the network $\Gamma(5, 7, 0)$. Solid red lines with full circles and with diamonds represent $\mathcal{E}(|V_D|)$ obtained in (9) with, respectively, $K_{\min} = 32$ and $K = 66$ resonances. The horizontal solid line denotes $\chi = |V| - |E| = -2$ (see (2)), the horizontal thick dashed lines specify the $\mathcal{E}(|V_D|)$ values within the accuracy limit $\epsilon = \pm 1/4$, while the thin dashed lines specify the maximum error $\epsilon = \pm 1/2$ that still allows the correct determination of $\mathcal{E}(|V_D|)$. The zero point on the x axis corresponds to the $\mathcal{E}(|V_D|)$ value calculated for the complete spectrum (no loss of resonances). The point 1 on the x axis corresponds to the $\mathcal{E}(|V_D|)$ value obtained when the first resonance was lost. The next points correspond to the $\mathcal{E}(|V_D|)$ values obtained for the lost resonances with the consecutive numbers in the energy spectrum. In Fig. 5, we show the numerical results for the complete graph $\Gamma(8, 28, 0)$. The generalized Euler characteristic $\mathcal{E}(|V_D|)$ was calculated using $K_{\min} = 563$ resonances in (9). The horizontal solid line denotes $\chi = |V| - |E| = -20$. The remaining markings are the same as in Fig. 4.

As we see, the changes are dramatic. For both graphs the loss of the lowest energy levels leads to $\mathcal{E}(|V_D|)$ values which differ from its expected value by more than $|1/2|$. Although the quantitative results differ, the changes of $\mathcal{E}(|V_D|)$ are of the same nature. It should be noticed that for both graphs the values of the maximum deviations from the expected values of $\mathcal{E}(|V_D|)$ are quite similar. In fact,

one should expect such a behavior since in the calculation of $\mathcal{E}(|V_D|)$ using (9) a single term with the same number n is removed. For example, for the graphs $\Gamma(5,7,0)$ and $\Gamma(8,28,0)$ for $n=1$, the values of k_1/t_0 are 1.12 and 0.98 leading to the departure from $\mathcal{E}(|V_D|)$ by 1.68 and 1.74, respectively. Moreover, as it is clearly seen in Fig. 4, increasing the number of resonances in (9), $K \gg K_{\min}$, does not change this situation. Also the boundary conditions do not influence this dependence.

Thus, the possibility of obtaining the generalized Euler characteristic $\mathcal{E}(|V_D|)$ of a graph/network in two independent ways, from the pure topological feature of the graph/network and from its spectrum, makes it a perfect indicator of lost low energy levels.

5. Summary

There is no doubt that the possibility of calculating the generalized Euler characteristic $\mathcal{E}(|V_D|)$ on the basis of the graph/network spectrum and comparing it with the Euler characteristic χ defined by its pure topological properties opens a new window in the experimental investigation of the microwave networks and quantum graphs simulated by them. In this article we show that using the generalized Euler characteristic $\mathcal{E}(|V_D|)$ it is possible to determine the number of vertices with Dirichlet and Neumann boundary conditions, even in the complex graphs. This is an extension of our previous findings published in [18]. We also show that the generalized Euler characteristic $\mathcal{E}(|V_D|)$ evaluated from the spectra of the graphs can serve as an excellent indicator of missing resonances in the low energy range.

Acknowledgments

This work was supported in part by the National Science Centre, Poland, Grants No. 2016/23/B/ST2/03979 and No. 2018/30/Q/ST2/00324, the Swedish Research Council (Grant 2020-03780) and the Center for Interdisciplinary Research (ZiF) in Bielefeld in the framework of the cooperation group on *Discrete and continuous models in the theory of networks*.

References

[1] L. Euler, *Comment. Acad. Sci. U. Petrop* **8**, 128 (1741), written in 1735.

[2] L. Pauling, *J. Chem. Phys.* **4**, 673 (1936).

[3] D. Kowal, U. Sivan, O. Entin-Wohlman, Y. Imry, *Phys. Rev. B* **42**, 9009 (1990).

[4] Y. Imry, *Introduction to Mesoscopic Physics*, Oxford 1996.

[5] J. A. Sanchez-Gil, V. Freilikher, I. Yurkevich, A.A. Maradudin, *Phys. Rev. Lett.* **80**, 948 (1998).

[6] R. Mittra, S.W. Lee, *Analytical Techniques in the Theory of Guided Waves*, Macmillan, New York 1971.

[7] R.P. Feynman, *Phys. Rev.* **76**, 749 (1949).

[8] P. Exner, P. Šeba, P. Šťovíček, J. Phys. A **21**, 4009 (1988).

[9] T. Kottos, U. Smilansky, *Phys. Rev. Lett.* **79**, 4794 (1997).

[10] T. Kottos, U. Smilansky, Ann. Phys. **274**, 76 (1999).

[11] R. Blümel, Yu Dabaghian, R.V. Jensen, *Phys. Rev. Lett.* **88**, 044101 (2002).

[12] G. Berkolaiko, P. Kuchment, *Introduction to Quantum Graphs*, Mathematical Surveys and Monographs 186, 2013, p. 270.

[13] Z. Pluhař, H.A. Weidenmüller, *Phys. Rev. Lett.* **112**, 144102 (2014).

[14] L.K. Pinheiro, B.S. Souza, V. Trevisian, *Discussiones Mathematicae — Graph Theory* **40**, 607 (2020).

[15] P. Kurasov, *Arkiv för Matematik* **46**, 95 (2008).

[16] P. Kurasov, *J. Funct. Anal.* **254**, 934 (2008).

[17] M. Ławniczak, P. Kurasov, Sz. Bauch, M. Białous, V. Yunko, L. Sirko, *Phys. Rev. E* **101**, 052320 (2020).

[18] M. Ławniczak, P. Kurasov, S. Bauch, M. Białous, A. Akhshami, L. Sirko, *Sci. Rep. E* **11**, 15342 (2021).

[19] O. Hul, S. Bauch, P. Pakoński, N. Savytskyy, K. Życzkowski, L. Sirko, *Phys. Rev. E* **69**, 056205 (2004).

[20] M. Ławniczak, O. Hul, S. Bauch, P. Šeba, L. Sirko, *Phys. Rev. E* **77**, 056210 (2008).

[21] O. Hul, M. Ławniczak, S. Bauch, A. Sawicki, M. Kuś, L. Sirko, *Phys. Rev. Lett.* **109**, 040402 (2012).

[22] M. Ławniczak, S. Bauch, L. Sirko, in: *Handbook of Applications of Chaos Theory* eds. Christos Skiadas and Charilaos Skiadas, CRC Press, Boca Raton 2016, p. 559.

[23] B. Dietz, V. Yunko, M. Białous, S. Bauch, M. Ławniczak, L. Sirko, *Phys. Rev. E* **95**, 052202 (2017).

[24] M. Ławniczak L. Sirko, *Sci. Rep.* **9**, 5630 (2019).

[25] V. Yunko, M. Białous, L. Sirko, *Phys. Rev. E* **102**, 012210 (2020).

[26] J. Lipovský, *J. Phys. A* **49**, 375202 (2016).

[27] M. Ławniczak, J. Lipovský, L. Sirko, *Phys. Rev. Lett.* **122**, 140503 (2019).

[28] O. Hul, O. Tymoshchuk, S. Bauch, P.M. Koch, L. Sirko, *J. Phys. A* **38**, 10489 (2005).

[29] A. Rehemanjiang, M. Allgaier, C.H. Joyner, S. Müller, M. Sieber, U. Kuhl, H.-J. Stöckmann, *Phys. Rev. Lett.* **117**, 064101 (2016).

[30] M. Ławniczak, S. Bauch, O. Hul, L. Sirko, *Phys. Rev. E* **81**, 046204 (2010).

[31] M. Allgaier, S. Gehler, S. Barkhofen, H.-J. Stöckmann, U. Kuhl, *Phys. Rev. E* **89**, 022925 (2014).

[32] M. Białous, V. Yunko, S. Bauch, M. Ławniczak, B. Dietz, L. Sirko, *Phys. Rev. Lett.* **117**, 144101 (2016).

[33] M. Ławniczak, M. Białous, V. Yunko, S. Bauch, B. Dietz, L. Sirko, *Acta Phys. Pol. A* **132**, 1672 (2017).

[34] B. Dietz, T. Friedrich, H.L. Harney, M. Miski-Oglu, A. Richter, F. Schäfer, H.A. Weidenmüller, *Phys. Rev. E* **81**, 036205 (2010).

[35] J.-H. Yeh, Z. Drikas, J. Gil Gil, S. Hong, B.T. Taddese, E. Ott, T.M. Antonsen, T. Andreadis, and S.M. Anlage, **124**, 1045 (2013).

[36] X. Zheng, S. Hemmady, T.M. Antonsen, Jr.S.M. Anlage, E. Ott, *Phys. Rev. E*, **73** 046208 (2006).

[37] H.-J. Stöckmann, J. Stein, *Phys. Rev. Lett.* **64**, 2215 (1990).

[38] S. Sridhar, A. Kudrolli, *Phys. Rev. Lett.***72**, 2175 (1994).

[39] L. Sirko, P.M. Koch, R. Blümel, *Phys. Rev. Lett.* **78**, 2940 (1997).

[40] Y. Hlushchuk, A. Kohler, Sz. Bauch, L. Sirko, R. Blümel, M. Barth, H.-J. Stöckmann, *Phys. Rev. E* **61**, 366 (2000).

[41] Y. Hlushchuk, A. Błędowski, N. Savytskyy, L. Sirko, *Phys. Scr.* **64**, 192 (2001).

[42] Y. Hlushchuk, L. Sirko, U. Kuhl, M. Barth, H.-J. Stöckmann, *Phys. Rev. E* **63**, 046208 (2001).

[43] R. Blümel, P.M. Koch, L. Sirko, *Found. Phys.* **31**, 269 (2001).

[44] A. Dhar, D.M. Rao, U. Shankar, S. Sridhar, *Phys. Rev. E* **68,** 026208 (2003).

[45] N. Savytskyy, O. Hul, L. Sirko, *Phys. Rev. E* **70**, 056209 (2004).

[46] S. Hemmady, X. Zheng, E. Ott, T.M. Antonsen, S.M. Anlage, *Phys. Rev. Lett.* **94**, 014102 (2005).

[47] O. Hul, N. Savytskyy, O. Tymoshchuk, S. Bauch, L. Sirko, *Phys. Rev. E* **72**, 066212 (2005).

[48] B. Dietz, A. Richter, *Chaos* **25**, 097601 (2015).

[49] M. Białous, B. Dietz, L. Sirko, *Phys. Rev. E* **100**, 012210 (2019).

[50] B. Dietz, T. Klaus, M. Miski-Oglu, A. Richter, M. Wunderle, *Phys. Rev. Lett* **123**, 174101 (2019).

[51] R. Blümel, A. Buchleitner, R. Graham, L. Sirko, U. Smilansky, H. Walther, *Phys. Rev. A* **44**, 4521 (1991).

[52] R.V. Jensen, S.M. Susskind, M.M. Sanders, *Phys. Rep.* **201**, 1 (1991).

[53] M. Bellermann, T. Bergemann, A. Haffmann, P.M. Koch, L. Sirko, *Phys. Rev. A* **46**, 5836 (1992).

[54] L. Sirko, S. Yoakum, A. Haffmans, P.M. Koch, *Phys. Rev. A* **47**, R782 (1993).

[55] A. Buchleitner, D. Delande, *Phys. Rev. Lett.* **71**, 3633 (1993).

[56] L. Sirko, M.R.W. Bellermann, A. Haffmans, P.M. Koch, D. Richards, *Phys. Rev. Lett.* **71**, 2895 (1993).

[57] J.E. Bayfield, S.-Y. Luie, L.C. Perotti, M.P. Skrzypkowski, *Physica D: Nonlinear Phenomena* **83**, 46 (1995).

[58] L. Sirko, P.M. Koch, *Appl. Phys. B* **60**, S195 (1995).

[59] L. Sirko, A. Haffmans, M.R.W. Bellermann, P.M. Koch, *Europhys. Lett.* **33**, 181 (1996).

[60] J. Bayfield, Lal Pinnaduwage, *J. Phys. B* **18**, L49 (1999).

[61] L. Sirko, S.A. Zelazny, P.M. Koch, *Phys. Rev. Lett.* **87**, 043002 (2001).

[62] L. Sirko, P.M. Koch, Phys. *Rev. Lett.* **89**, 274101 (2002).

[63] A. Arakelyan, J. Nunkaew, T.F. Gallagher, *Phys. Rev. A* **94**, 053416 (2016).

[64] M. Ławniczak, P. Kurasov, S. Bauch, M. Białous, L. Sirko, in: *13th Chaotic Modeling and Simulation International Conference*, Springer Proceedings in Compplexity 551, 2021.

[65] M. Ławniczak, P. Kurasov, S. Bauch, M. Białous, L. Sirko, *Acta Phys. Pol. A* **139**, 323 (2021).

[66] M. Ławniczak, S. Bauch, V. Yunko, M. Białous, J. Wrochna, L. Sirko, *Acta Phys. Pol. A* **136**, 811 (2019).

[67] D.S. Jones, *Theory of the Electromagnetism*, Pergamon Press, Oxford 1964.

[68] N. Savytskyy, A. Kohler, Sz. Bauch, R. Blümel, L. Sirko, *Phys. Rev. E* **64**, 036211 (2001).

[69] M. Białous, B. Dietz, L. Sirko, *Phys. Rev E* **103**, 052204 (2021).

[70] O. Bohigas, M.P. Plato, *Phys. Lett. B* **595** 171 (2004).

[71] M. Ławniczak, M. Białous, V. Yunko, S. Bauch, L. Sirko, *Phys. Rev E* **98**, 012206 (2018).